

# Probing Hard Scattering Processes via Multiple Weak Gauge Boson Production at the Future Colliders

Ijaz Ahmed,<sup>1,\*</sup> M. S. Amjad,<sup>2,†</sup> Farzana Ahmad,<sup>3,‡</sup> and Jamil Muhammad<sup>4,§</sup>

<sup>1</sup>*Federal Urdu University of Arts, Science and Technology, Islamabad, Pakistan*

<sup>2</sup>*National University of Technology, Islamabad, Pakistan*

<sup>3</sup>*SERI, & College of Engineering, Konkuk University, Seoul 05029, South Korea*

<sup>4</sup>*Sang-Ho College of Education, Konkuk University, Seoul 05029, Korea*

(Dated: March 16, 2026)

## Abstract

One of the possible ways to detect new physics phenomena particles is to investigate the weak gauge boson production resulting from hadron-hadron scattering. This study comprises the production of multiple weak gauge bosons as a result of hard scattering between proton-proton beams at multi-TeV energies with an integrated luminosity of  $\mathcal{L} = 3000 \text{ fb}^{-1}$ . The effective production cross-sections for pair, triple, and quartic scattering mechanisms have been computed as a function of  $\sqrt{s}$ . The center-of-mass energy has been varied from 8 TeV to 100 TeV to encompass future collider capabilities. Among all studied processes, the triple scattering process  $W^+W^-W^+$  has been selected as the signal process based on its dominant cross-section. The background channels— $ZZZ$ ,  $ZZZZ$ ,  $W^-ZZ$ ,  $W^+ZZ$ ,  $W^+W^-Z$ ,  $W^+W^-ZZ$ ,  $W^+W^-W^+W^-$ —which have comparatively lower cross-sections, have been considered from possible scattering mechanisms to investigate the effect of higher luminosity on low production cross-section processes. Different decay modes have been analyzed. For both lepton- and hadron-specific decays of W and Z bosons, the cumulative efficiencies for each signal and background process have been computed. This study demonstrates an effective methodology for background suppression through systematic optimization of the signal-to-background ratio. The results indicate that, despite the lower cross-sections of higher-order scattering processes, their distinctive kinematic features enable effective signal isolation at future colliders.

PACS numbers:

Keywords:

---

\*Electronic address: [Ijaz.Ahmed@fuuast.edu.pk](mailto:Ijaz.Ahmed@fuuast.edu.pk)

†Electronic address: [sohailamjad@nutech.edu.pk](mailto:sohailamjad@nutech.edu.pk)

‡Electronic address: [farzana@konkuk.ac.kr](mailto:farzana@konkuk.ac.kr)

§Electronic address: [mjamil@konkuk.ac.kr](mailto:mjamil@konkuk.ac.kr)

## I. INTRODUCTION

The Standard Model of particle physics (SM) gives a sufficient explanation of three basic particle interactions. It encompasses two additional theories, electroweak theory [1] and quantum chromodynamics (QCD) [2]. However, there are multiple unanswered questions, including gravity [3], dark matter, matter-antimatter asymmetry, sterile neutrino oscillations [4], etc. Therefore, it is considered incomplete [5]. An endeavor to find New Physics or Physics beyond the Standard Model has been going on for multiple decades. A possible avenue to discover the new particles is through multiple weak gauge boson production and by studying the scattering of bosons produced as a result of hadron-hadron collisions [6]. In this recent study, we address this aspect, which has not been frequently studied, although there do exist some previous efforts in this regard, such as [7–10, 30]. Recent roadmaps for high-energy frontiers highlight the importance of multi-boson processes at 100 TeV and Muon Colliders [33]. Current feasibility studies for the Future Circular Collider (FCC-hh) highlight its potential for exploring the high-energy limits of the electroweak sector [37], while future lepton colliders offer unique precision in determining gauge-Higgs coupling structures [40]. Furthermore, the observation of triboson production at 13 TeV by the ATLAS and CMS collaborations has opened new windows into testing the electroweak sector [31]. Most recently, the observation of  $WZ\gamma$  and rigorous searches for  $WZZ$  and  $ZZZ$  final states have significantly extended the sensitivity of the Standard Model to rare multi-boson interactions [35, 36].

The specific objectives of this study are: (i) to compute and analyze the production cross-sections for pair, triple, and quartic gauge boson scattering across a broad energy spectrum (8 TeV to 100 TeV), (ii) to investigate the kinematic distributions of leptonic and hadronic decay modes to identify distinguishing features between signal and background processes, and (iii) to evaluate the signal significance and signal-to-background ratios at high luminosities ( $\mathcal{L} = 3000 fb^{-1}$ ) by applying optimized kinematic cuts. While the  $W^+W^-W^+$  process is calculated here within the Standard Model (SM) framework, it serves as a critical baseline for New Physics searches. Specifically, triple boson production is highly sensitive to Anomalous Quartic Gauge Couplings (aQGCs), where any deviation from the SM prediction would signal BSM physics. Furthermore, the  $W^+W^-W^+$  process acts as a primary irreducible background for exotic searches, such as the production of doubly charged Higgs particles ( $pp \rightarrow H^{\pm\pm}W^\mp$ ) or searches for singly charged Higgs bosons. The investigation of multiple weak gauge boson production is not only a crucial test of the Standard Model (SM) electroweak symmetry breaking but also serves as a sensitive probe

for physics beyond the Standard Model (BSM). At the energy scales of future 100 TeV colliders, the triple-boson processes computed in this work act as the primary irreducible background for exotic searches, such as the production of doubly charged Higgs bosons ( $H^{\pm\pm} \rightarrow W^\pm W^\pm$ ) or heavy resonance decays. By establishing high-precision SM benchmarks across a wide energy spectrum (8–100 TeV), this study provides the necessary baseline to identify deviations that would signal Anomalous Quartic Gauge Couplings (aQGCs) or other effective field theory (EFT) effects in the electroweak sector. Therefore, a precise understanding of these multi-boson processes is essential to distinguish potential new physics signals from the standard electroweak continuum. Any statistically significant deviation from the SM cross-sections or the kinematic distributions presented in this study would provide direct evidence of Beyond Standard Model (BSM) effects in the electroweak symmetry breaking sector. Keeping such a scenario in mind, in this work, we have examined the pair, the triple, and the quartic scatterings of the W and Z bosons. All these calculations are carried out using the standard model parameters. For all the possible scattering mechanisms, cross-sections are computed by varying collision energies from 8 TeV to 100 TeV. Particularly, the two decay modes, i.e., the hadronic and the leptonic decay of W and Z bosons, are considered. For lepton-specific decays, the W bosons decay as  $W^{\pm} \rightarrow l^{\pm}\nu$  while the Z boson decays into a pair of lepton and anti-lepton  $Z \rightarrow l^-l^+$ . For the hadronic decay mode, both W and Z bosons decay into a pair of jets  $Z/W^\pm \rightarrow jj$ . The background processes have been suppressed using various kinematic cuts. For lepton-specific decays, we have plotted transverse momentum  $P_T$ , number of leptons  $N$ , missing transverse energy  $E_T$ , mass  $M_T$ , pseudorapidity  $\eta$ , and the azimuthal angle  $\Delta\phi$ . For these variables, the cuts are  $P_T > 10$  GeV,  $|\eta| < 3$ . For the hadron-specific decays, we have also computed the reconstructed mass  $M$  and hadronic energy  $H_T$ . The applied cuts are,  $P_T > 20$  GeV,  $|\eta| < 3$ , and  $H_T > 600$  GeV. After applying each cut, the cumulative efficiencies for each decay mode and for each process are tabulated. The background contribution from off-shell Higgs production ( $H^* \rightarrow ZZ/WW$ ) is effectively suppressed by our selection criteria. Specifically, the requirement of  $H_T > 600$  GeV for hadronic channels and the focus on triple-boson final states shifts the analysis phase space significantly above the Higgs resonance and its immediate off-shell tail, where the continuum multi-boson production becomes the dominant contributor. Due to each cut, the efficiency reduces compared to the previous value. In this final study, signal-to-background ratio  $S/B$  and other signal significance  $S/\sqrt{B}$  and  $S/\sqrt{S+B}$  are also computed at the integrated luminosity  $\mathcal{L} = 3000$   $fb^{-1}$ . For the hadronic decay, the significance ratio  $S/\sqrt{B}$  reduces from 13.69 to 11.82, whereas  $S/\sqrt{S+B}$  gradually decreases from 10.19 to 8.46 after applying the cuts on various parameters. To ensure the experimental relevance of this analysis,

the kinematic selection criteria employed—specifically the lepton transverse momentum  $P_T > 10$  GeV and pseudorapidity  $|\eta| < 3.0$ —are designed to be consistent with the baseline acceptance and trigger thresholds utilized in current ATLAS and CMS multi-boson searches at 13 TeV [7, 8]. Furthermore, these parameters are extrapolated to the 100 TeV Future Circular Collider (FCC-hh) environment, where similar central-region requirements are expected to suppress pile-up and beam-induced backgrounds [28]. Furthermore, the implementation of optimized event selection strategies, including machine-learning-assisted clustering, is becoming essential for distinguishing multi-boson signals from the vast QCD backgrounds at these future facilities [38].

## II. ANALYSIS SETUP AND TOOLS

The computational analysis follows a structured multi-stage workflow to ensure precision and reproducibility. Matrix element calculation and initial event generation are performed using the MadGraph5\_aMC@NLO framework [11]. To ensure high physical accuracy, including finite-width effects and full spin correlations in the decay chains, the final-state gauge bosons are treated as off-shell particles rather than using a narrow-width approximation. These generated events, stored in standard LHE format, are then interfaced with FastJet [13] for jet clustering. For the hadronic decay modes, the anti- $k_t$  algorithm with a radius parameter of  $R = 0.4$  is employed to reconstruct jets from the final-state partons. The subsequent analysis phase, including the application of kinematic selection cuts and the calculation of physical observables (such as  $p_T$ ,  $\eta$ , and  $M_T$ ), is conducted via MadAnalysis5 [12]. Finally, the ROOT analysis package [14] is utilized for statistical interpretation and data visualization. The reliability of this setup was validated through internal consistency checks, such as gauge invariance tests, and by benchmarking our simulated cross-sections against established Standard Model results at  $\sqrt{s} = 13$  and 14 TeV, showing excellent agreement.

The reliability of this computational setup was validated through several internal consistency checks. We performed gauge invariance tests for all multi-boson processes and verified that the results remained stable. Furthermore, we benchmarked our simulated cross-sections against established Standard Model results at  $\sqrt{s} = 13$  and 14 TeV, finding excellent agreement with previous literature. Technical advancements, such as CPU vectorization and GPU-based offloading, have also been integrated into the framework to handle the increasing complexity of multi-particle phase space calculations efficiently [32, 39]. Technical advancements, such as CPU vectorization and GPU-based offloading, have also been integrated into the framework to handle the increasing complexity of multi-particle phase space calculations efficiently [32, 39]. It is important to clarify

the implementation of the  $ZZZ$  and  $WZZ$  channels within the MadGraph5 framework. While a triple- $Z$  vertex is forbidden at tree-level in the Standard Model (SM),  $ZZZ$  production is generated via  $t$ -channel quark exchange diagrams (e.g.,  $q\bar{q} \rightarrow ZZZ$ ). Our analysis remains strictly within the SM framework, and no anomalous triple gauge couplings (aTGCs) were introduced, ensuring the results represent a conservative SM baseline. In the next step, such events are analyzed by using MadAnalysis [12]. The jet clustering and its reconstruction are carried out with the FastJet [13] interface. After that, the output is analyzed by the ROOT analysis package [14]. This investigation is separated into two sections, covering the leptonic and hadronic decay channels of the weak gauge bosons. In particular, the following weak boson production modes are analyzed:

- Double boson scattering
  - $pp \rightarrow ZZ$  and  $pp \rightarrow W^+W^-$
  - For like-charged Gauge boson Pairs, jets are added to avoid Isospin violation.  
 $pp \rightarrow W^+W^+jj$  and  $pp \rightarrow W^-W^-jj$ .
- Triple boson scattering
  - $pp \rightarrow ZZZ$ , and  $pp \rightarrow W^+W^-W^+$
  - $pp \rightarrow W^+W^-Z$ ,  $pp \rightarrow W^+ZZ$ ,  $pp \rightarrow W^-ZZ$ ,  $pp \rightarrow ZZZ$
- Quartic boson scattering
  - $pp \rightarrow W^+W^-W^+W^-$   $pp \rightarrow ZZZZ$ , and  $pp \rightarrow W^+W^-ZZ$

In addition, we are going to investigate and analyze the production modes of the parameters like production cross section as a function of center of mass energy  $\sigma(\sqrt{s})$ , pseudorapidity  $\eta$ , lepton multiplicity  $N(\textit{lepton})$  (for leptonic decays only), Lepton transverse momentum  $p_T$  (for leptonic decays only), lepton transverse mass  $M_T$  (for leptonic decays only), missing transverse energy  $E_T$  (for leptonic decays only), hadronic energy  $H_T$  (for hadronic decays only) and invariant mass of jets (for hadronic decays only)

### III. RESULTS AND DISCUSSION

The production cross-sections governing pair and triple scattering mechanisms exhibit rapid scaling behavior, rising sharply as a direct function of the increasing center-of-mass energy. While

the rate of increase begins to soften as  $\sqrt{s}$  approaches the 100 TeV regime due to the logarithmic evolution of parton distribution functions (PDFs), the absolute cross-sections continue to grow significantly, as evidenced by the logarithmic scale in Figure 1, providing substantial event yields for quartic processes at future facilities. It is worth noting that the change in behavior after 30 TeV is very similar for all the scattering bosons.

The possible Feynman diagrams for the multiple gauge boson production processes are illus-

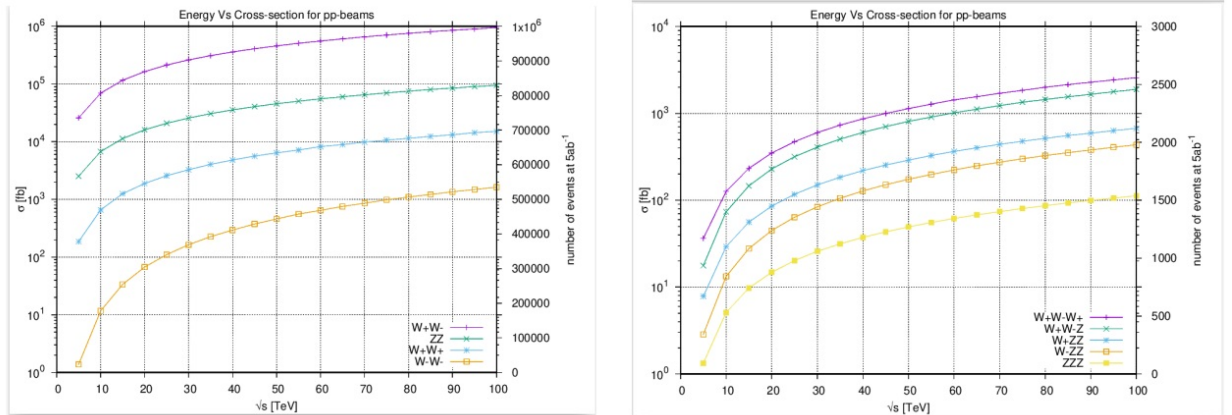


FIG. 1: The dependence of the production cross section on the center of mass energy is shown for double (left) and triple (right) boson scattering.

trated in Figure 2. Following the generation of these events, we analyze the resulting kinematic distributions. Figure 3 presents the transverse momentum ( $p_T$ ) and transverse mass ( $M_T$ ) of the leptons generated from these decays. The transverse mass ( $M_T$ ) distributions for processes involving  $W$  bosons, such as  $WZZ$  and  $W^+W^-W^+$ , exhibit a characteristic Jacobian peak near 80 GeV, corresponding to the  $W$  boson mass. This peak is analytically determined by the kinematic relation:

$$M_T = \sqrt{2p_T^\ell E_T^{miss}(1 - \cos \Delta\phi_{\ell,\nu})} \quad (1)$$

where  $p_T^\ell$  is the transverse momentum of the lepton,  $E_T^{miss}$  is the missing transverse energy from the neutrino, and  $\Delta\phi_{\ell,\nu}$  is the azimuthal angle between them. The concentration of events near  $M_W$  occurs because the  $M_T$  distribution is bounded from above by the mass of the parent particle ( $M_T \leq M_W$ ), creating a sharp kinematic edge that serves as a vital signature for identifying leptonic  $W$  decays amidst the background. The transverse mass ( $M_T$ ) distributions for processes involving  $W$  bosons, such as  $WZZ$  and  $W^+W^-W^+$ , exhibit a characteristic Jacobian peak near 80

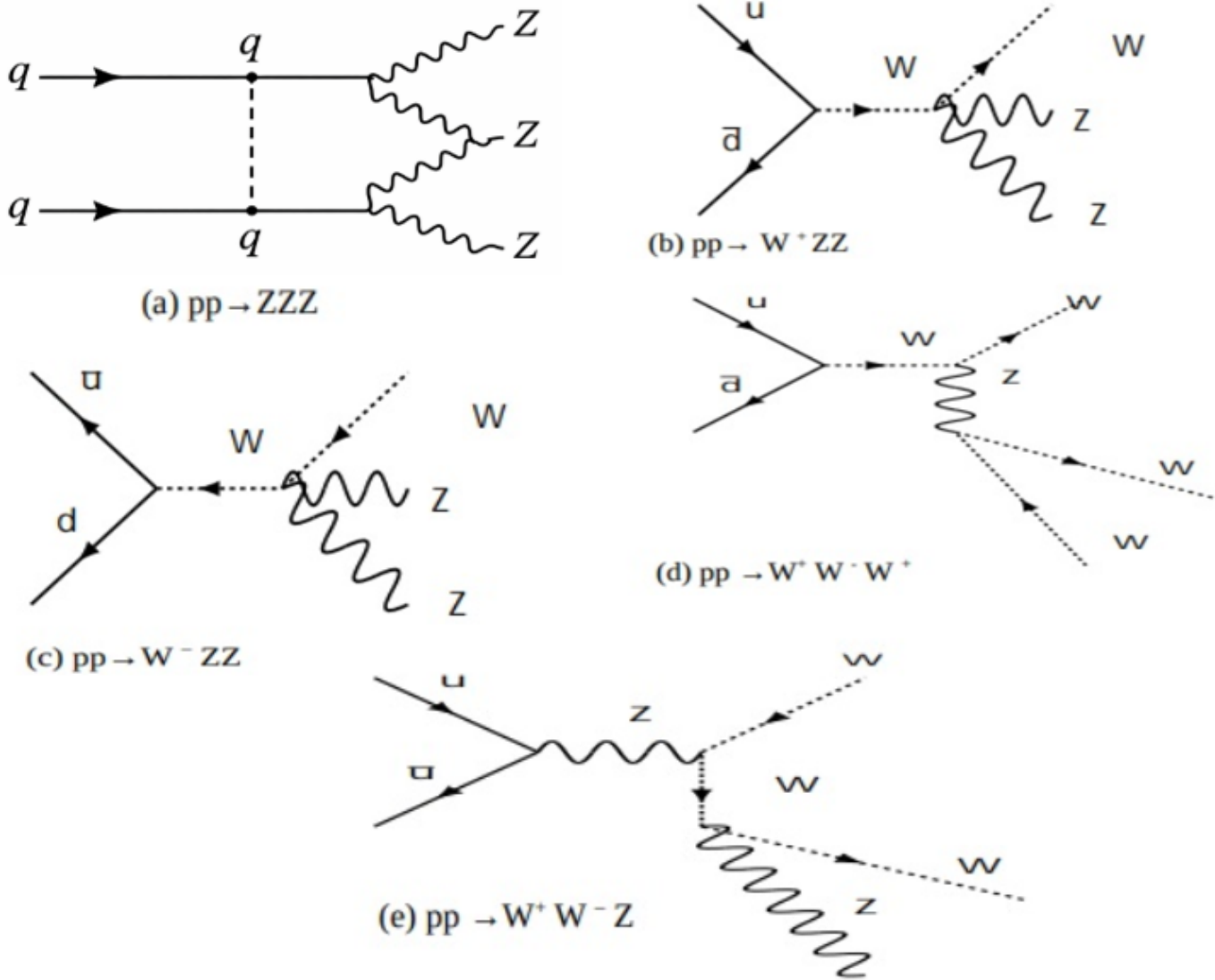


FIG. 2: A view of the possible Feynman diagrams for multiple gauge boson production.

GeV, corresponding to the  $W$  boson mass. This peak is analytically determined by the kinematic relation  $M_T = \sqrt{2p_T^\ell E_T^{miss}(1 - \cos \Delta\phi_{\ell,\nu})}$ , where  $p_T^\ell$  is the transverse momentum of the lepton,  $E_T^{miss}$  is the missing transverse energy from the neutrino, and  $\Delta\phi_{\ell,\nu}$  is the azimuthal angle between them. The concentration of events near  $M_W$  occurs because the  $M_T$  distribution is bounded from above by the mass of the parent particle ( $M_T \leq M_W$ ), creating a sharp kinematic edge that serves as a vital signature for identifying leptonic  $W$  decays amidst the background.

We can see that the triple boson scattering where only one  $W$  is present with two  $Z$  bosons behaves a bit differently as compared to the other modes. Furthermore, the overall trend for both of these variables remains the same for the different kinds of scattering over the range of  $p_T$  and

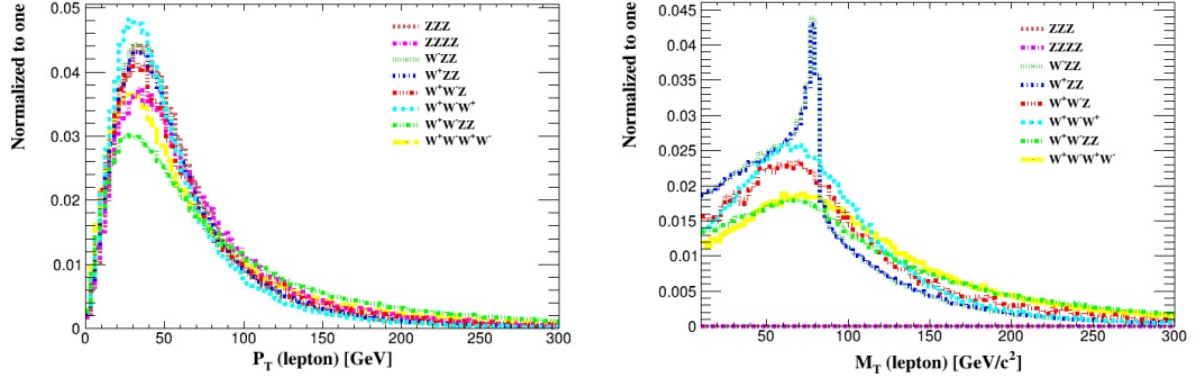


FIG. 3: The transverse momentum  $p_T$  (left) and mass  $M_T$  (right) are shown for the lepton-specific decay modes.

$M_T$ . However, we do observe a difference in the peak for different scattering channels, where the reconstructed momentum peak seems to be lower for the quartic scatterings.

Our investigation proceeds to the analysis of missing transverse energy. This kinematic signature arises from the emission of invisible neutrinos during the leptonic decay channels of charged  $W$  bosons, a process that is analyzed via the missing energy distributions in Figure 4. We observe the variation in pattern for the reconstructed  $E_T$  based on the number and type of bosons being analyzed. The single  $W$  channels have a clear peak with the right tail, while the two or more  $W$  boson channels show a larger spread of neutrino energy. Figure 4 illustrates the missing transverse energy ( $E_T$ ) and pseudorapidity for the signal and background processes. While  $E_T$  primarily arises from neutrinos in  $W$  decays, we include the  $ZZZ$  and  $ZZZZ$  backgrounds to demonstrate their relative contribution; in these neutral channels,  $E_T$  signatures result from  $Z \rightarrow \nu\nu$  decay modes or detector resolution effects modeled in the reconstruction. The differing peak heights and tail extensions indicate that quartic and triple scattering processes exhibit broader energy dispersion compared to pair production, a feature that aids in distinguishing complex multi-boson events from simpler backgrounds.

To validate our computational framework, we benchmarked our simulated cross-sections at  $\sqrt{s} = 13$  and 14 TeV against existing experimental measurements and Standard Model (SM) predictions from the ATLAS and CMS collaborations. Specifically, our results for diboson ( $ZZ$ ) and triboson ( $WWW$ ) production show a high degree of consistency with measured values reported in Ref. [7, 8, 31], accounting for differences in center-of-mass energy and fiducial phase space. As shown in Table IV, the differences between the experimental measurements (which include higher-order corrections) and our Leading Order (LO) simulations are consistent with expected theoretical K-

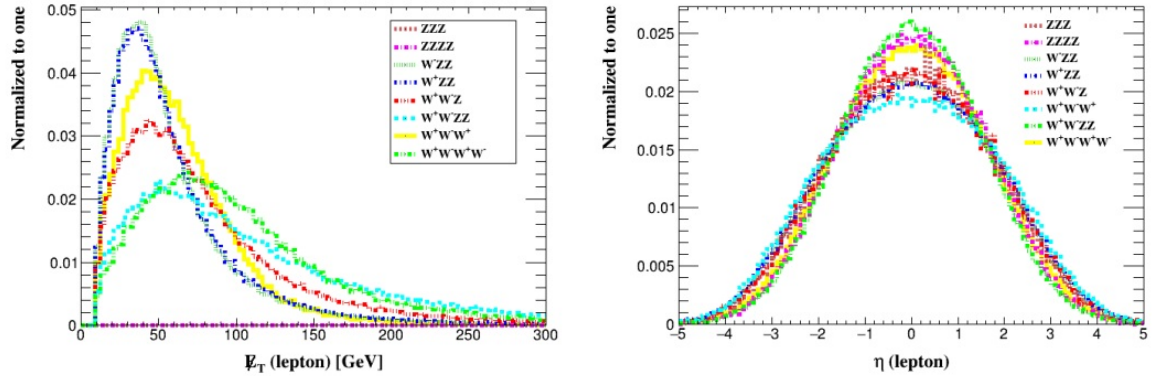


FIG. 4: The missing transverse energy (left) and pseudorapidity for the single leptonic decay of the W bosons.

factors.

TABLE I: Comparison of experimental measurements at  $\sqrt{s} = 13$  TeV with simulated Leading Order (LO) results at  $\sqrt{s} = 14$  TeV.

Process	Exp. Result (13 TeV)	This Work (LO, 14 TeV)	Reference
$ZZ$	$17.3 \pm 0.9$ pb	$10.3 \pm 0.12$ pb	ATLAS [7]
$W^+W^-$	$115.8 \pm 6.3$ pb	$64.6 \pm 0.17$ pb	CMS [7]
$W^+W^-W^+$	$820 \pm 130$ fb*	$78.8 \pm 0.02$ fb	ATLAS [31]

\*Note: Experimental result [31] represents the total  $WWW$  cross-section, while this study simulates the specific  $W^+W^-W^+$  charge state.

### A. Pair of Weak Gauge Boson Production

Whenever the multiple partons interact, they exchange momentum and reach higher energy levels because the maximum flux of partons is observed. The probability of Parton Pair Scattering with hadron interactions was anticipated a long time ago [15–17]. However, at CERN, the AFS collaboration provided evidence for double scattering in proton-proton collisions [18, 19]. Moreover, this process was observed at the Fermi lab by Collider Detector by considering the final states of the particles [20]. If two or more parton pairs scatter independently in hadronic collisions, multiple parton scattering occurs [21]. This double scattering examines the correlation between partons and hadrons in the transverse plane by providing more information about the hadronic structure. The parton-parton correlation can be neglected if the scattering event is parameterized by high energy.

The dependence of the production cross-section on the center-of-mass energy was evaluated for the scattering of weak gauge boson pairs.

Table II displays the cross-sections for the weak gauge boson pair using the different energy ranges. For each process, a cross-section is calculated between the energy range 8 TeV and 100 TeV. The expected error is also computed for each process. FD represents the possible Feynman diagrams for each process. However, jets are added to avoid isospin violation for like-charged Gauge boson Pairs. Further, the jets are the light quarks too. In particle physics, a jet is generally produced by the hadronization of quarks or gluons by making a narrow cone.

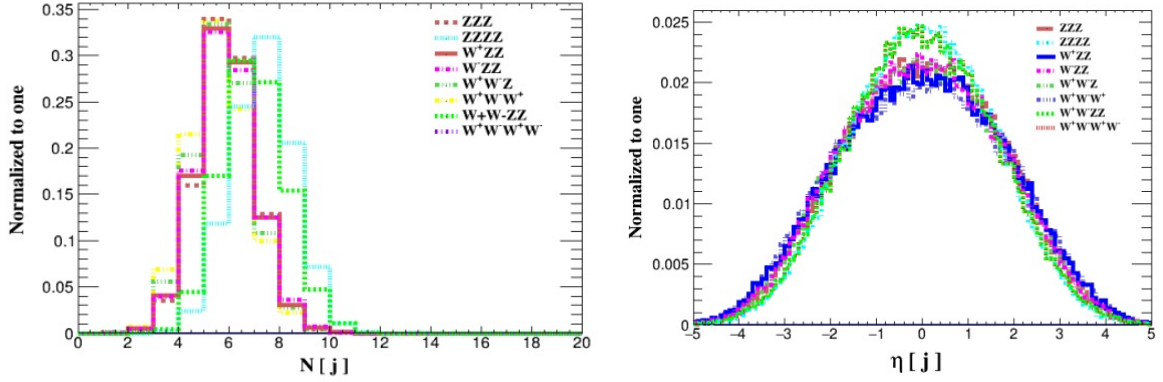


FIG. 5: (left) A distribution of jet multiplicity for hadron-specific decay of all gauge bosons. (Right) The plot shows the pseudorapidity distribution of jets for signal and all background processes.

TABLE II: The cross-sections for pair weak gauge bosons for various energy ranges.

Process	8 TeV $\sigma[pb] \pm error$	14 TeV $\sigma[pb] \pm error$	27 TeV $\sigma[pb] \pm error$	100 TeV $\sigma[pb] \pm error$	F.D
ZZ	$4.803 \pm 0.0114$	$10.3 \pm 0.122$	$23.02 \pm 0.0053$	$98.36 \pm 0.0237$	10
$W^+W^-$	$34.15 \pm 0.080$	$64.62 \pm 0.168$	$154.3 \pm 0.292$	$637.2 \pm 1.451$	10
$W^+W^- jj$	$0.08206 \pm 0.002$	$0.2153 \pm 0.0006$	$0.584 \pm 0.021$	$2.9 \pm 0.120$	11
$W^+W^- jj$	$0.0307 \pm 0.0005$	$0.09548 \pm 0.002$	$0.3017 \pm 0.007$	$2.05 \pm 0.006$	11

TABLE III: The cross-sections along with varying energy for the triple scattering mechanism.

Process	8 TeV $\sigma[pb] \pm error$	14 TeV $\sigma[pb] \pm error$	27 TeV $\sigma[pb] \pm error$	100 TeV $\sigma[pb] \pm error$	F.D
ZZZ	0.0042±0.0009	0.01028± 0.005	0.02672±0.0006	0.1357± 0.003	42
$W^-ZZ$	0.0357± 0.006	0.014± 0.005	0.02966±0.005	0.162± 0.0032	28
$W^+ZZ$	0.0075± 0.008	0.01844± 0.005	0.0499±0.0001	0.227± 0.0006	36
$W^+W^-W^+$	0.03404 ± 0.008	0.07877 ±0.022	0.1922 ±0.006	0.9201 ± 0.001	40

TABLE IV: The cross-sections for the quartic scattering mechanism along with varying energy.

Process	8 TeV $\sigma[pb] \pm error$	14 TeV $\sigma[pb] \pm error$	27 TeV $\sigma[pb] \pm error$	100 TeV $\sigma[pb] \pm error$	F.D
ZZZZ	$5.88 \times 10^{-6} \pm 0.001$	$1.87 \times 10^{-5} \pm 0.004$	$6.03 \times 10^{-5} \pm 0.0001$	$3.8 \times 10^{-3} \pm 0.00015$	192
$W^+W^-ZZ$	$1.1 \times 10^{-4} \pm 0.0006$	$4.2 \times 10^{-4} \pm 0.0001$	$4.3 \times 10^{-4} \pm 0.0002$	$0.0106 \pm 0.0003$	426
$W^+W^-W^+W^-$	$1.5 \times 10^{-4} \pm 0.001$	$4.9 \times 10^{-4} \pm 0.0001$	$\{1.6 \times 10^{-3} \pm 0.0005$	$0.0103 \pm 0.00042$	592

### B. Triple Parton Scattering of Weak Gauge Boson

In the standard model [22], the approximations of cross-section and cms energy for three weak gauge bosons have been performed. Table II shows the cross-sections along with varying energy for the triple scattering mechanism. For each process, a cross-section is calculated between energy ranges 8 TeV and 100 TeV. The expected error is also computed for each process. In this Table, FD represents the possible Feynman diagrams for each process.

Table III displays the cross-sections for the quartic scattering mechanism along with varying energy at cms. The cross-sections for the quartic scattering mechanism are the processes along with the errors that are computed. All these calculations showed that by increasing the center of mass energy, the cross-section of various scattering mechanisms increases rapidly. A sharp increase can be seen graphically.

### C. Pseudorapidity

It is the angle between the particle and the beam axis [23], [24]. It has one-to-one correspondence with the polar angle  $\theta$ . It can be expressed as:

$\eta = -\ln[\tan(\theta/2)]$  where  $\theta$  is the angle between the three components of momentum and the positive beam axis. The particles with  $\eta = 0$  are along the beam axis, while the particles having large pseudorapidity are lost. Kinematic cuts  $|\eta| < 3$  are used to suppress the background. Figure 5 displays the pseudorapidity for leptonic decays.

#### D. Multiplicity

Multiplicity refers to the number of particles present in a specific process for a specific center of mass energy in a certain decay [25]. Here, in Figure 5, the lepton multiplicity is plotted. W and Z bosons have extremely short lifetimes of approximately  $\sim 10^{-25}$  s, decaying into quarks and leptons with distinct branching fractions. Specifically, the W boson decays into a charged lepton-neutrino pair about 33% of the time, with the remaining 67% resulting in hadronic states. In contrast, the Z boson yields hadrons 70% of the time, neutrinos 20% of the time, and charged lepton pairs approximately 10% of the time. For both bosons, the hadronic decay modes are notably challenging to identify due to the overwhelming dijet background, which is orders of magnitude higher [34]. Table IV depicts the cumulative efficiencies for each background and signal processes for the lepton-specific decay at cms energy 14 TeV. The cumulative efficiency for each process is defined as the ratio of events surviving a specific cut to the total number of events initially generated. Physically, it represents the survival probability of the signal or background at each stage of the selection process, allowing us to quantify the rejection power of our kinematic requirements.

Table IV depicts the cumulative efficiencies for each background and signal processes for the lepton-specific decay at cms energy 14 TeV. The cumulative efficiency for each process is defined as the ratio of events surviving a specific cut to the total number of events initially generated. Physically, it represents the survival probability of the signal or background at each stage of the selection process, allowing us to quantify the rejection power of our kinematic requirements. The calculated cross-sections for both signal and background events are summarized in the Table. Additionally, we define  $P_T$  as the transverse momentum associated with the leptonic decays of W and Z bosons, imposing a kinematic threshold of  $P_T > 10$  GeV. As neutrinos remain unaffected by some interactions, there exists missing transverse energy for which the cuts  $E_T > 80$  GeV are applied.

The effective cross-sections for Z boson triple and quartic scattering are very low, so applying the kinematic cuts on transverse momentum, the numbers for efficiency reduce, whereas by applying missing transverse energy and pseudorapidity cuts, their values almost reduce to zero. The rest of

the processes show variation in efficiencies by applying kinematic cuts. Upon applying kinematic cuts of  $P_T > 10$  GeV ,  $E_T > 80$  GeV and  $|\eta| < 3$ , we calculated the significance and S/B ratios, which are presented in Table V.

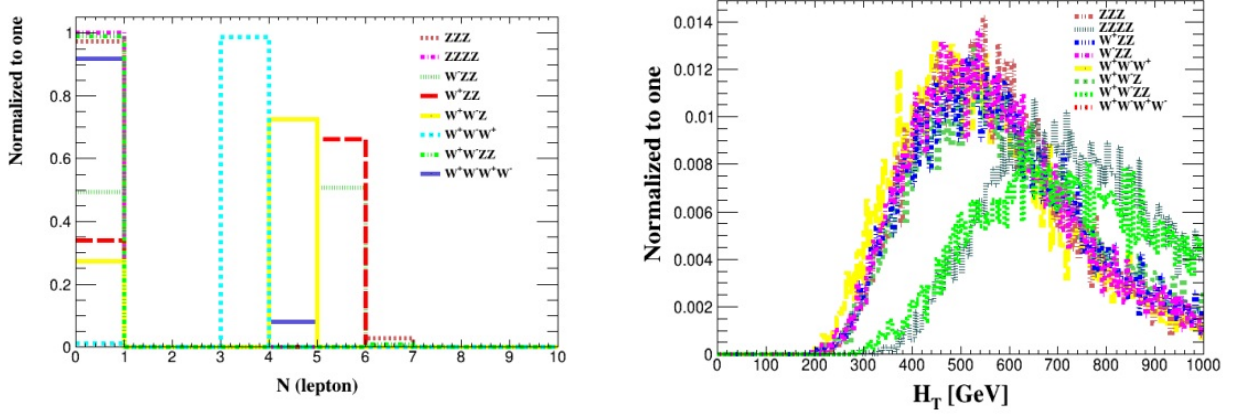


FIG. 6: The Lepton multiplicity for various Decays of weak gauge bosons at the left side, while the view of the distribution of the Hadronic Energy (HT) in the Hadron-specific decay at the right side.

TABLE V: The cumulative efficiencies for each background and signal processes for lepton-specific decay at cms energy 14 TeV.

Triple Boson Scattering					
	$ZZZ$	$W^-ZZ$	$W^+ZZ$	$W^+W^-Z$	$W^+W^-W^+$
$\sigma[pb]$	$3.1 \times 10^{-6}$	$1.03 \times 10^{-5}$	$1.96 \times 10^{-5}$	$3.0 \times 10^{-4}$	$8.4 \times 10^{-3}$
$P_T > 10$ GeV	$0.2 \pm 0.24$	$(0.50 \pm 0.15) \times 10^{-5}$	$0.6 \pm 0.11$	$0.96 \pm 0.1$	$0.99 \pm 0.004$
Quartic Boson Scattering					
	$ZZZZ$	$W^+W^-ZZ$	$W^+W^-W^+W^-$		
$\sigma[pb]$	$4.9 \times 10^{-10}$	$9.32 \times 10^{-9}$	$1.28 \times 10^{-8}$		
$P_T > 10$ GeV	$4 \times 10^{-5} \pm 0.32$	$9 \times 10^{-4} \pm 0.3$	$0.081 \pm 0.24$		

### E. Hadronic decays

Since W and Z bosons possess hadronic decay channels, we reconstructed the invariant masses of the resulting jets to analyze these specific modes. The corresponding cross-sections for these

processes, calculated at various energy points, are summarized in Table IV for the leptonic mode and Table VI for the hadronic mode. In the analysis of hadronic decays, we designated the  $W^+ W^- W^+$  channel as the signal, treating all other interactions as background. Since  $W$  and  $Z$  bosons possess hadronic decay channels, we reconstructed the invariant masses of the resulting jets to analyze these specific modes. The corresponding cross-sections for these processes, calculated at various energy points, are summarized in Table IV for the leptonic mode and Table VI for the hadronic mode. In the analysis of hadronic decays, we designated the  $W^+W^-W^+$  channel as the signal, treating all other interactions as background. The pseudorapidity distributions in Figure 5 (right) show that jets from multi-boson production are highly central, peaking at  $\eta \approx 0$ . This is a crucial distinguishing feature from  $t$ -channel background processes, which tend to be more forward-peaked. By applying a cut of  $|\eta| < 3$ , we retain the majority of the signal while significantly suppressing SM noise.

The other observables are also plotted for the hadron-specific decays. Instead of missing transverse energy, the hadronic energy distribution is plotted as shown in Figure 6. Similarly, the jet multiplicity  $N(j)$ , which shows the number of jets present in each process, is also computed as shown in Figure 6(a). Moreover, the pseudorapidity of jets for hadron-specific decay is estimated and presented in Figure 6(b). Furthermore, the  $H_T$  distribution in Figure 6 confirms that the signal events are characterized by high energy deposits, justifying the  $H_T > 600$  GeV threshold to isolate hard scattering from soft QCD backgrounds.

#### IV. INVARIANT MASS

The invariant mass is generated with the possible jet pairs. It can be computed using the chi-square method, which is a standard statistical approach for mass reconstruction in high-energy physics [26, 27]:

$$\chi^2 = \frac{\sum (W_{rec,i} - 80.5)^2}{\sigma_{jets}^2} \quad (2)$$

where  $W_{rec,i}$  represents the reconstructed mass of the  $i$ -th jet pair identified during the event analysis, and 80.5 GeV is the reference nominal mass of the  $W$  boson used for the minimization fit. The parameter  $\sigma_{jets}$  denotes the jet energy resolution of the detector system, representing the measurement uncertainty associated with hadronic showers.

We calculate the reconstructed invariant mass of the multi-boson system using the expression

below:

$$m_{inv}^2 = E^2 - |P|^2 \quad (3)$$

In Eq. (2),  $m_{inv}$  is the invariant mass,  $E$  represents the total energy (the scalar sum of energies of reconstructed particles), and  $|P|$  is the magnitude of the total three-momentum vector, derived from the vector sum of the momentum components of all final-state decay products. The plots for the invariant mass distributions are presented in Figure 7.

Table V, shows the signal significance ratios of signals and backgrounds for leptonic decay. While Table VI presents the cumulative efficiencies for both signal and background events. These results reflect the application of specific selection cuts designed to minimize background channels. As detailed in Table V, the impact of kinematic cuts on the signal-to-background ratio is significant. We observe that applying the  $P_T > 10$  GeV cut yields an S/B ratio of approximately 2.19. While stricter cuts on Missing  $E_T (> 80)$  and pseudorapidity ( $|\eta| < 3$ ) result in a decrease in the raw signal count to 1966.8 events, the statistical significance  $S/\sqrt{B}$  remains robust at approximately 59. This confirms that even after rigorous background suppression, the signal remains statistically observable at an integrated luminosity of  $3000 \text{ fb}^{-1}$ .

The results presented in the final column of Table V ( $S/\sqrt{S+B}$ ) represent the total statistical significance of the signal. It is noteworthy that even after the most stringent kinematic requirements ( $|\eta| < 3$ ), the significance remains at 35.486, which is substantially higher than the  $5\sigma$  discovery threshold. This indicates that the triple-boson signal is highly robust against the considered backgrounds at future high-luminosity colliders. Furthermore, we acknowledge that this analysis is performed at Leading Order (LO). One-loop QCD and electroweak (EW) corrections for multi-boson processes typically introduce K-factors that can increase the total cross-sections by 10% – 30%, depending on the specific center-of-mass energy and the order of the process. While these higher-order corrections would likely enhance the absolute signal yields and thus improve the statistical significance further, the fundamental kinematic shapes (such as the Jacobian peaks) and the relative efficiency of our optimized selection cuts are expected to remain stable. Therefore, the background suppression strategy and the feasibility conclusions presented here remain valid and conservative.

A close look at Table VII shows that the selection cut of transverse momentum of jets  $P_T > 20$  has been applied. For the hadronic energy, we have also applied a cut that is  $H_T < 600$ . By applying various kinematic cuts, the value for the S/B ratio decreases (as tabulated in Table VII)

as one process is chosen to be the signal and the rest of them as backgrounds so it is important to compute their signal-to-background ratio. By applying cuts, the signal-to-background ratio ( $S/B$ ) reduces. After application of various cuts, the rest of the signal significance ratios also reduce. For instance, here in this Table, when no cuts are applied, the signal is 234. However, after applying the cut, its value reduces to 145.64. The significance ratio  $S/\sqrt{B}$  reduces from 13.69 to 11.82, whereas  $S/\sqrt{S+B}$  gradually decreases from 10.19 to 8.46 after applying cuts on various parameters. The significance plots are also constructed, and signal-to-background ratios are computed for each process at the luminosity of  $3000 \text{ fb}^{-1}$ .

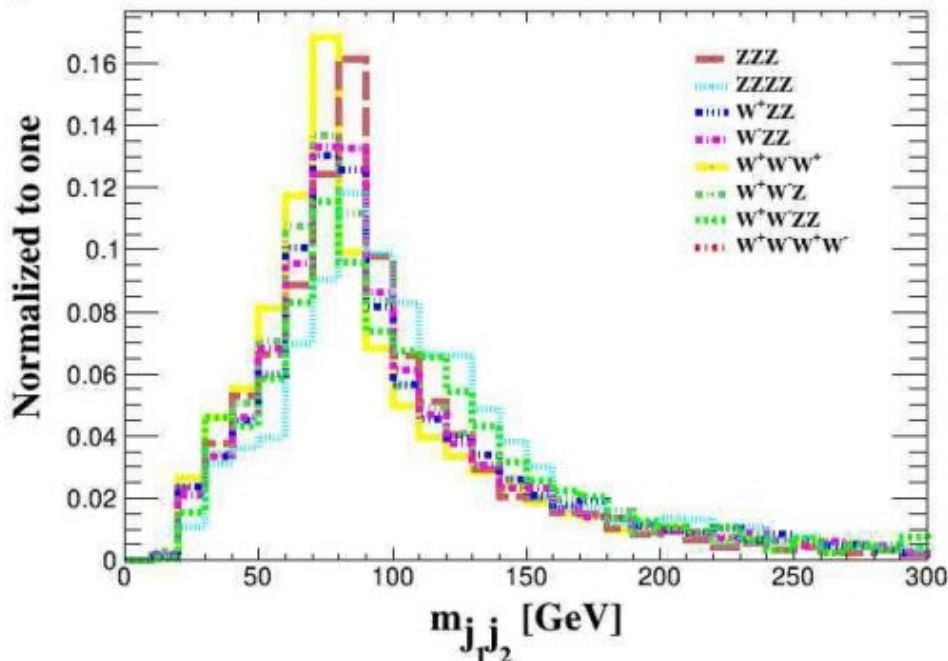


FIG. 7: The view of the invariant mass distribution of jet pair.

## V. CONCLUSION

The primary scope of this research was to scrutinize the generation of multiple weak gauge bosons arising from high-energy proton-proton interactions. This analysis is conducted within the projected experimental environment of the Large Hadron Collider (LHC), assuming a center-of-mass energy of  $\sqrt{s} = 14 \text{ TeV}$  and a target integrated luminosity of  $3000 \text{ fb}^{-1}$ . The calculations of cross-sections at the center of mass energy 100 TeV for future colliders are also estimated. In this analysis,  $W^+W^-W^+$  is assumed as a signal and the rest of them as the background channels. We

TABLE VI: The signal significance ratios of signals and backgrounds for leptonic decays at  $L \sim 3000 fb^{-1}$  and  $\sqrt{s} = 14$  TeV.

Cuts	Signal	Background	S/B	$S/\sqrt{B}$	$S/\sqrt{S+B}$
No cuts	$8437.41 \pm 7.12$	$3331.2 \pm 2.6$	$2.5328 \pm 0.002$	$146.1878 \pm 0.0023$	$77.776 \pm 0.043$
$P_T > 10$ GeV	$6297.7 \pm 40.3$	$2876.8 \pm 8.9$	$2.1891 \pm 0.020$	$117.41611 \pm 0.001$	$65.749 \pm 0.285$
$E_T > 80$ GeV	$1968.8 \pm 38.9$	$1105.5 \pm 26.9$	$1.7809 \pm 0.055$	$59.21308 \pm 0.0072$	$35.508 \pm 0.501$
$ \eta  < 3$	$1966.8 \pm 38.9$	$1105.2 \pm 26.9$	$1.7796 \pm 0.055$	$59.16244 \pm 0.0072$	$35.486 \pm 0.501$

TABLE VII: The cumulative efficiency for the hadronic decay of weak gauge bosons.

Triple Boson Scattering					
	ZZZ	$W^- ZZ$	$W^+ ZZ$	$W^+ W^- Z$	$W^+ W^- W^+$
$\sigma [pb]$	0.00155	0.00192	0.00367	0.0218	0.0218
$P_T(j) > 20$ GeV	$0.13 \pm 0.08$	$0.14 \pm 0.08$	$0.99 \pm 0.01$	$0.99 \pm 0.01$	$0.99 \pm 0.004$
Quartic Boson Scattering					
	ZZZZ	$W^+ W^- ZZ$	$W^+ W^- W^+ W^-$		
$\sigma [pb]$	$1.58 \times 10^{-6}$	0.00011	0.00011		
$P_T(j) > 20$ GeV	$0.31 \pm 3.6$	$0.41 \pm 0.47$	$0.4 \pm 0.47$		

TABLE VIII: The signal-to-background ratio for each process in the hadronic decay.

Cuts	Signal	Background	S/B	$S/\sqrt{B}$	$S/\sqrt{S+B}$
No cuts	234.0	291.0	0.0804	13.7	10.2
$N(j) \geq 6$	$232.95 \pm 1.14$	$289.20 \pm 1.44$	$0.80526 \pm 0.0056$	$13.69621 \pm 0.0017$	$10.1937 \pm 0.0413$
$ \eta (j) < 3$	$232.86 \pm 1.18$	$289.19 \pm 1.47$	$0.80521 \pm 0.0057$	$13.69310 \pm 0.0017$	$10.1915 \pm 0.0427$
$H_T < 600 GeV$	$145.64 \pm 7.42$	$150.25 \pm 8.51$	$0.9693 \pm 0.0738$	$11.882 \pm 0.019$	$8.467 \pm 0.347$

have successfully characterized the kinematic behaviors of these channels, particularly highlighting the discriminating power of missing transverse energy and invariant mass distributions.

We have summarized that our finalized plots for each variable are in good agreement with the actual

values. The analytical framework presented herein is designed to serve as a pivotal resource for future investigations into the production of multiple weak gauge bosons within the Standard Model context. Based on current simulation data, the prospects for detection are highly encouraging; specifically, the chosen parameters for center-of-mass energy and integrated luminosity provide sufficient sensitivity to successfully observe all the theoretical scenarios hypothesized in this study. The calculated significances suggest that the  $W^+W^-W^+$  channel will be accessible in the High-Luminosity LHC era, providing a vital test of the electroweak sector. Our results could be quite useful for researchers working in the field of multiple weak gauge bosons.

Our results indicate that a 100 TeV collider provides an unparalleled environment for multi-boson physics. Compared to recent HL-LHC projections [6, 29], which are limited by the partonic energy fraction, our study demonstrates that the triple-boson signal significance remains robust even after rigorous background suppression. This confirms that future facilities can reach the precision required to test the quartic gauge couplings of the electroweak sector with high statistical confidence.

Crucially, the cross-sections and kinematic distributions presented here define the 'Standard Model ceiling' for future high-energy frontiers. At an integrated luminosity of  $3000 \text{ fb}^{-1}$ , our results provide a quantitative reference for the expected SM yields, enabling future studies to calculate the statistical significance of potential BSM signals. If future experimental data at 100 TeV shows an excess of events beyond the benchmarks provided in Tables I–III, it would constitute definitive evidence for new physics—such as aQGCs or heavy resonances—that cannot be explained within the current Standard Model framework.

## VI. ACKNOWLEDGMENT

## VII. STATEMENTS AND DECLARATIONS

**Funding:** The authors confirm that this work was conducted without any specific funding, grants, or financial assistance.

**Competing Interests:** The authors declare that they have no competing interests, financial or otherwise .

- 
- [1] T. W. B. Kibble, “History of electroweak symmetry breaking,” J. Phys. Conf. Ser. **626**, No.1, 012001 (2015).
- [2] I. J. R. Aitchison and A. J. G. Hey, “Gauge Theories in Particle Physics: A Practical Introduction, Volume 2: Non-Abelian Gauge Theories,” (CRC Press, 2012).
- [3] V. C. De Andrade and J. G. Pereira, “Gravitational Lorentz force and the description of the gravitational interaction,” Phys. Rev. D **56**, 4689 (1997).
- [4] J. Kopp, P. A. N. Machado, M. Maltoni, and T. Schwetz, “Sterile neutrino oscillations: the global picture,” JHEP **2013**, 5, 1-52 (2013). DOI: 10.1007/JHEP05(2013)050 & Arxiv.org/abs/1303.3011v3
- [5] J. R. Johnson, “Does a Theory of Everything Exist?,” Philosophy and Cosmology **26**, 132-147 (2021).
- [6] M. Gallinaro et al., “Beyond the Standard Model in vector boson scattering signatures,” arXiv:2005.09889 [hep-ph] (2020).
- [7] A. Oh, “Measurements of multi vector boson production processes at the LHC,” Prog. Part. Nucl. Phys. **108**, 103708 (2019). Doi.org/10.1016/j.pnpnp.2019.06.002
- [8] “Measurement of double parton scattering in same-sign WW production in p-p collisions at  $\sqrt{s} = 13TeV$ ” with the CMS experiment, CMS Collaboration 2017, CMS-PAS-FSQ-16-009.
- [9] M. Y. Hussein, Multiple Weak Gauge Boson production at the LHC as a probe of hard scattering processes,” Quark Confinement and the Hadron Spectrum V, pp. 484-488 (2003). doi.org/10.1142/9789812704269\_0096.
- [10] D. A. Morris, “Prospects for Multiple Weak Gauge Boson Production at Supercollider Energies,” Workshop on Physics at Current Accelerators and the Supercollider, 0061-72. arxiv.org/pdf/hep-ph/9308326v1.
- [11] J. Alwall et al., “The automated computation of tree-level and NLO differential cross sections, and their matching to parton shower simulations,” JHEP **2014**, 7, 079 (2014). DOI:10.1007/JHEP07(2014)079
- [12] E. Conte, B. Fuks, and G. Serret, “MadAnalysis 5, a user-friendly framework for collider phenomenology,” Comput. Phys. Commun. **184**, 222-256 (2013).
- [13] (a) M. Cacciari, G. P. Salam, and G. Soyez, “FastJet user manual”, Eur. Phys. J. C **72**, 1896 (2012). & “FastJet: a code for fast kt clustering, and more,” <https://arxiv.org/abs/hep-ph/0607071>.
- [14] R. Brun and F. Rademakers, “ROOT - An Object-Oriented Data Analysis Framework,” Nucl. Instrum. Meth. A **389**, 81-86 (1997).
- [15] E. Huayra, E. G. de Oliveira, and R. Pasechnik, ”Probing double parton scattering via associated open charm and bottom production,” Eur. Phys. J. C **79**, 880 (2019).
- [16] J. R. Andersen et al., ”Exploring high-purity multi-parton scattering at hadron colliders,” arXiv:2307.05693 [hep-ph] (2024).
- [17] T. Kasemets and M. Diehl, ” Angular correlations in the double Drell-Yan process”” JHEP 2013, 121, (2013). DOI:10.1007/JHEP01(2013)121

- [18] D. Cockerill et al., "Performance of the AFS-Vertex Detector at the CERN ISR," *Phys. Scripta* **23**, 649 (1981).
- [19] O. Botner et al., "Performance of the AFS vertex detector at the CERN ISR," *Nucl. Instrum. Meth.* **196**, 315-318 (1982).
- [20] F. Abe et al. [CDF Collaboration], "Measurement of double parton scattering in  $p\bar{p}$  collisions at  $\sqrt{s} = 1.8$  TeV," *Phys. Rev. D* **56**, 3811-3832 (1997).
- [21] H. Abramowicz et al., "Summary of the workshop on multi-parton interactions (MPI@LHC 2012)," arXiv:1306.5413 [hep-ph] (2013).
- [22] Giampiero Passarino, Christian Sturm Sandro Uccirati, "Complete Electroweak Corrections to Higgs production in a Standard Model with four generations at the LHC", *Phys. Lett. B* 706 (2011) 195-199. DOI: 10.1016/j.physletb.2011.11.012
- [23] D. H. Perkins, *Introduction to High Energy Physics*, 4th Edition, Cambridge University Press, 2000.
- [24] Z. Jiang et al., "Hydrodynamic description of pseudorapidity distributions of charged particles in p-p collisions," *Chin. J. Phys.* **54**, 371-378 (2016).
- [25] (a) D. A. Morris, "Prospects for multiple weak gauge boson production," UCLA-93-TEP-30 (1993).  
(b) D. A. Morris, "Prospects for Multiple Weak Gauge Boson Production at Supercollider Energies" arxiv.org/abs/hep-ph/9308326.
- [26] G. Cowan, *Statistical Data Analysis*, Oxford University Press, 1998.
- [27] R. L. Workman et al. [Particle Data Group], "Review of Particle Physics," *Prog. Theor. Exp. Phys.* **2022**, 083C01 (2022).
- [28] FCC Collaboration, "FCC-hh: The Hadron Collider Conceptual Design Report," *Eur. Phys. J. ST* **228**, no.4, 755-1107 (2019). DOI: 10.1140/epjst/e2019-900087-0.
- [29] Raffaele Angelo Gerosa, Milan Bicocca and Milan Bicocca U., "Vector Boson Scattering prospects for High-Luminosity LHC at CMS in the same sign WW final state", CMS Collaboration, PoS Lepton-Photon2015 (2016) **111**.
- [30] Christopher Schwan, "Vector boson scattering at the LHC," PoS RADCOR 2017 (2018) 081. Doi.org/10.22323/1.290.0081
- [31] G. Aad, ATLAS Collaboration, "Observation of WWW production in pp collisions at 13 TeV with the ATLAS Detector," *Phys. Rev. Lett.* **129**, 061803 (2022). DOI: 10.1103/PhysRevLett.129.061803.
- [32] Carlo Flore, Daniel Kikoła, Aleksander Kusina, Jean-Philippe Lansberg, Olivier Mattelaer & Anton Safronov, "Automated NLO calculations for asymmetric hadron-hadron collisions in *MadGraph5\_aMC@NLO*," *Eur. Phys. J. A*, **61**, 239, (2025). DOI: 10.1140/epja/s10050-025-01707-1
- [33] K. R. Long et al., "Muon colliders to expand frontiers of particle physics," *Nature Phys.* **17**, 289-292 (2021). DOI: 10.1038/s41567-020-01130-x
- [34] S. Navas et al. (Particle Data Group), "Review of Particle Physics," *Phys. Rev. D* **110**, 030001 (2024).
- [35] CMS Collaboration, "Observation of WZ production and constraints on new physics scenarios in proton-proton collisions at  $\sqrt{s} = 13$  TeV" ', *Phys. Rev. D* **109**, 012001 (2024). arXiv:2503.21977

- [36] ATLAS Collaboration, "Observation of  $WZ\gamma$  production in  $pp$  collisions at  $\sqrt{s} = 13$  TeV with the ATLAS detector," *Phys. Rev. Lett.* **132**, 021802 (2024).
- [37] M. Benedikt et al., "The Future Circular Collider: Feasibility Study status and prospects," *Eur. Phys. J. ST* **233**, 1-15 (2024) DOI: 10.1140/epjs/s11734-025-01967-4.
- [38] Shuai Zhang, Ji-Chong Yang & Yu-Chen Guo., "Using k-means assistant event selection strategy to study anomalous quartic gauge couplings at muon colliders," *Eur. Phys. J. C* **84**, 142 (2024). DOI: 10.1140/epjc/s10052-024-12494-2.
- [39] Andrea Valassi, et al., "Speeding up MadGraph5\_aMC@NLO through CPU vectorization and GPU offloading: towards a first alpha release" arXiv:2303.18244 [hep-ph] (2023).
- [40] C. H. de Lima and D. Tuckler, "Sign of gauge-Higgs boson couplings at future lepton colliders," *Phys. Rev. D* **111**, 015021 (2025). DOI:10.1103/PhysRevD.111.015021